PROCEEDINGS OF SCIENCE

Gravitational waves from the first order electroweak phase transition in the Z_3 symmetric singlet scalar model *

Toshinori Matsui†
School of Physics, KIAS, Seoul 02455, Korea
E-mail: matsui@kias.re.kr

Among various scenarios of baryon asymmetry of the Universe, electroweak baryogenesis is directly connected with physics of the Higgs sector. We discuss spectra of gravitational waves which are originated by the strongly first order phase transition at the electroweak symmetry breaking, which is required for a successful scenario of electroweak baryogenesis. In the Z_3 symmetric singlet scalar model, the significant gravitational waves are caused by the multi-step phase transition. We show that the model can be tested by measuring the characteristic spectra of the gravitational waves at future interferometers such as LISA and DECIGO.

Corfu Summer Institute 2017 'School and Workshops on Elementary Particle Physics and Gravity'
2-28 September 2017
Corfu, Greece

*This proceeding paper is based on Ref. [1] in collaborated with Zhaofeng Kang and Pyungwon Ko.
†Speaker.

PoS(CORFU2017)092

1. Introduction

In the scenario of electroweak baryogenesis (EWBG) [2, 3], the strongly first order electroweak phase transition (SFOEWPT) is required to satisfy the condition of the departure from thermal equilibrium

$$\langle h\rangle_*/T_* \gtrsim 1, \tag{1.1}$$

with T_* being the temperature of EWPT and $\langle h\rangle_*$ the vacuum expected value (VEV) of the SM Higgs field h at T_*. In order to satisfy this condition, the extended Higgs sector from standard model (SM) is required. These extensions could help to build a barrier between the EW vacuum and a metastable vacuum at tree or loop level [3, 4]. The mechanism to generate a thermal cubic term for h by a tree level barrier is most easily implemented in the extended Higgs sectors by a singlet S, containing effective tree-level cubic terms $\sim S^3 + S|H|^2$ with H the SM Higgs doublet [5, 6, 7, 8, 9, 10, 11].

If the extended Higgs sector respects some symmetry such as Z_2, under which $S \to -S$ and $H \to H$, an alternative way to the desired tree level barrier is available in the symmetric limit where S does not acquire VEV at the present universe [7, 12, 13, 14, 15, 16]. Such a scenario is associated with multi-step PT's. The universe may have been once in the intermediate phase $\Omega_{\rm meta}$ and then tunneled through a tree level barrier to the phase $\Omega_{\rm EW}$, recovering the Z_2 symmetry.

We expect that gravitational wave (GW) is available to explore the nightmare scenario which is a case that the model cannot be tested at colliders. In principle, EWPT of $T_* \simeq 100$ GeV can be detectable at the GW observation experiments [17]. The space-based interferometers: LISA [18], DECIGO [19] and BBO [20], designed to be sensitive to GW density $\Omega_{\rm GW}h^2 \gtrsim 10^{-16} - 10^{-10}$ (depending on frequency $\simeq 10^{-3} - 10^{-1}$ Hz), will be launched in the near future [17].

2. Z_3 symmetric singlet scalar model

We introduce an isospin complex singlet scalar S transforming as $S \to e^{i2w}S$ with $w = \pi/3$ under Z_3, while the SM fields including the SM Higgs doublet H are neutral under Z_3. The most general renormalizable and Z_3-symmetric scalar potential $V(H,S)$ is given by

$$V_0(H,S) = -\mu_h^2|H|^2 - \mu_s^2|S|^2 + \lambda_h|H|^4 + \lambda_s|S|^4 + \lambda_{sh}|H|^2|S|^2 + \sqrt{2}\left(\frac{A_s}{3}S^3 + h.c.\right). \tag{2.1}$$

Compared to the Z_2-symmetric model, there is just one more parameter describing the cubic term $A_s S^3$, and it will give rise to distinguishable difference from the Z_2-symmetric model. We discuss later the possibility of S as a dark matter (DM) candidate [21]. After EWSB, two scalar fields are parametrized as $H = (G^+, (v + h^0 + iG^0)/\sqrt{2})$ and $S = (s^0 + ia_s^0)/\sqrt{2}$. There appear two physical degrees of freedom h and s in addition to Nambu-Goldstone modes $G^\pm$ and G^0 that are absorbed by the $W^\pm$- and Z^0-bosons. The vacuum stability condition reads as $\lambda_s > 0$, $\lambda_h > 0$ and $4\lambda_s\lambda_h > \lambda_{sh}^2$. At zero temperature $T = 0$, the model parameters are fixed to be $\lambda_h = m_h^2/(2v^2)$, $\mu_h^2 = m_h^2/2$ and $\mu_s^2 = \lambda_{sh}v^2/2 - m_s^2$ up to radiative corrections with v which is the VEV of h. Here, m_h and m_s are the physical masses of h and s. We use $v = 246$ GeV, $m_h = 125$ GeV, m_s, λ_s, λ_{sh} and A_s as the input parameters.

Expanding the scalar fields around their classical backgrounds, $\langle H\rangle = (0, \varphi_h/\sqrt{2})$ and $\langle S\rangle = \varphi_s/\sqrt{2}$, the one-loop effective potential at finite temperature is given by

$$V_{\rm eff}(\varphi_h,\varphi_s,T) = V_0(\langle H\rangle,\langle S\rangle) + \sum_i n_i \frac{M_i^4(\varphi_h,\varphi_s,T)}{64\pi^2}\left(\ln\frac{M_i^2(\varphi_h,\varphi_s,T)}{Q^2} - c_i\right) + \sum_i n_i \frac{T^4}{2\pi^2} I_{B,F}\left(\frac{M_i^2(\varphi_h,\varphi_s,T)}{T^2}\right) \quad (2.2)$$

where Q is the renormalization scale, which is set at v in our analysis. Here, n_i and $M_i(\varphi_\Phi,\varphi_S,T)$ denote the degrees of the freedom and the field-dependent masses for particles i, respectively. We consider loop contributions from the fields $i = h^0, s^0, a_s^0, G^\pm, G^0, W_{T,L}^\pm, Z_{T,L}, \gamma_{T,L}, t$ and b. We take the $\overline{\rm MS}$ scheme, where the numerical constants c_i are set at $3/2$ $(5/6)$ for scalars and fermions (gauge bosons). The thermally corrected field-dependent masses for the CP-even/odd, Goldstone, the weak gauge bosons and top quarks are given by, for example, Ref. [1, 22]. The contribution of the finite temperature is defined by $I_{B,F}(a^2) = \int_0^\infty dx\, x^2 \ln\left[1 \mp \exp\left(-\sqrt{x^2+a^2}\right)\right]$ for boson and fermions, respectively.

3. Characteristic parameter of gravitational waves from first order phase transition

For a given scalar potential $V_{\rm eff}(\vec{\varphi},T)$ with $\vec{\varphi}$ denoting a vector of real scalar fields in the multi dimensional fields space, the (critical) bubble can be found by extremizing the Euclidean action $S_E(T) \equiv S_3(T)/T$ where $S_3(T)$ is defined as $S_3(T) \equiv \int d^3x \left[(\partial\vec{\varphi})^2/2 + V_{\rm eff}(\vec{\varphi},T)\right]$. Then, the bubble nucleation rate per unit volume per unit time will be given by $\Gamma(t) = \Gamma_0(t)\exp[-S_E(t)]$ with the pre-factor $\Gamma_0 \sim T^4$. In order for the nucleated vacuum bubbles to percolate through the whole Universe, the nucleation rate per Hubble volume per Hubble time should reach the unity $\Gamma/H^4|_{T=T_*} \simeq 1$, which determines the transition temperature T_*.

The GW spectrum from first order phase transition (FOPT) can be parameterized by several parameters, with the most crucial two, α and β, which capture the main features of FOPT dynamics and largely determine the features of GW spectrum. We will follow the conventions in Ref. [17]. The parameter $\alpha \equiv \varepsilon/\rho_{\rm rad}$ is the total energy budget of FOPT normalized by the radiative energy $\rho_{\rm rad} = (\pi^2/30)g_* T_*^4$ with $g_*(=108.75)$ being the relativistic degrees of freedom in the plasma at the PT temperature T_*. The liberated latent heat $\varepsilon = -(\Delta V + T\partial V/\partial T)|_{T_*}$, with ΔV the vacuum energy gap between two vacua. Another parameter β is defined by $\beta \equiv -dS_E/dt|_{t_*}$. We use the dimensionless parameter $\widetilde{\beta} \equiv \beta/H_*$, where $H_* \equiv 1.66\sqrt{g_*}T_*^2/m_{\rm pl}$ is the Hubble constant.

4. Numerical results in the Z_3-symmetric model

4.1 Parameter space with multi-step phase transition

We use the code `cosmoTransitions` [23] for numerical studies on PT in the Z_3 symmetric scalar Higgs sector in order to study the vacuum structure at finite temperature. Each path of the transition pattern and the metastable vacua at the intermediate stage of the model are shown in Fig. 1 (left). At $T = 0$, we are interested in the case where the EWSB but Z_3-preserving vacuum $\Omega_h \equiv (\langle h\rangle = v, 0)$ is the ground state, which may be accompanied by a metastable vacuum $\Omega_s \equiv (0, \langle s\rangle \neq 0)$ or $\Omega_{sh} \equiv (\langle h\rangle \neq 0, \langle s\rangle \neq 0)$. The presence of Ω_{sh} is a new aspect in the Z_3-symmetric model compared to the Z_2-symmetric model, and it will make possible three-step PT's in our model.

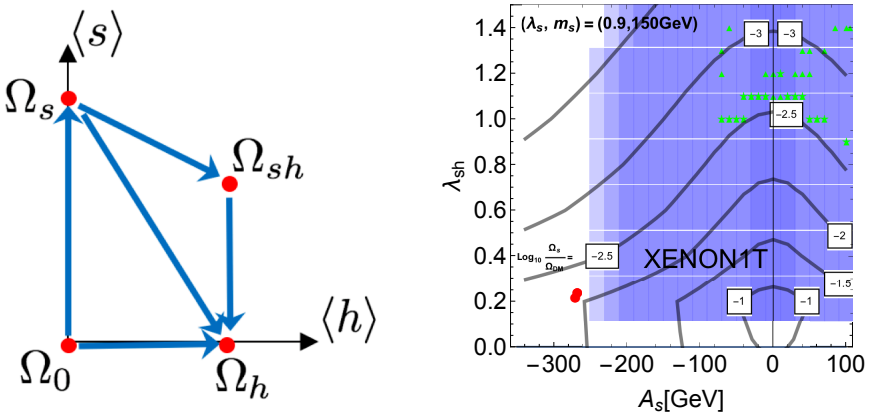

Figure 1: (Left) Patterns of the transition path and the metastable vacua at the intermediate stage in the Z_3 model. (Right) Types of multi-step PT in the (A_s, λ_{sh}) plane for $(\lambda_s, m_s[\mathrm{GeV}]) = (0.9, 150)$ as an example. PT of three-step (red, circle) and two-step (green, triangle for the second- $\to$ first- order PT or star for the first- $\to$ first- order PT) which satisfy the condition of SFOEWPT in Eq. (1.1) are plotted. The shaded blue regions are excluded by XENON1T [24]. The contours of the predicted thermal relic density of the model which is normalized by the observed one, $\log_{10}(\Omega_s/\Omega_{\mathrm{DM}})$, are plotted by the gray lines.

We summarize the parameter region of multi-step PT in Fig. 1 (right), where two-step PT and three-step PT are plotted [1]. In the $\mu_s^2 > 0$ region, we find that the two-step PT ($\Omega_0 \to \Omega_s \to \Omega_h$) can happen, with the first-step either second or first order, depending on the relevant parameters.

Two-step (second- $\to$ first- oder) PT case is basically corresponding to the Z_2-symmetric model in the $A_s \to 0$ limit, see the green triangle points in Fig. 1 (right). We found that A_s is restricted to be smaller than tens of GeV and thus the deviations are not significant for $\lambda_s \simeq 1$.

Two-step (first- $\to$ first- oder) PT for finite A_s, the first-step PT significantly becomes the FOPT shown as the green star points in Fig. 1 (right). In Fig. 2 (left) for a large $\lambda_s = 3$, the metastable Ω_s can be accommodated for much larger $A_s \sim \mathcal{O}(100)$ GeV. That large A_s, by contrast, is able to change the nature of transition $\Omega_0 \to \Omega_s$, into the first order type; furthermore, the strength of the second-step can be significantly enhanced and then reopens the smaller λ_{sh} region with $\lambda_{sh} \sim \mathcal{O}(0.1)$. We can find that the requirement $T_s^* \gtrsim T_h$ yields an upper bound on $|A_s| \lesssim 300$ GeV in this example. Note that the figures indicate that for a given A_s, the region for λ_{sh} is restricted and within this region increasing λ_{sh} could lead to lower T_h^*.

The three-step (first- $\to$ second- $\to$ first- oder) PT ($\Omega_0 \to \Omega_s \to \Omega_{sh} \to \Omega_h$) cases are shown as red circle points in Fig. 1 (right) which can happen only in a very narrow space for $\mu_s^2 < 0$ region. In Fig. 2 (right), we display the allowed region for $\lambda_{sh} = 0.24$ by taking the feasible values of (λ_s, m_s, A_s) in which we can find a point of Fig. 1 (right). Increasing λ_s lowers T_s^* and it will eventually go below T_h, thus shutting down the three-step PT. On the other hand, when λ_s becomes fairly small (thus for a much larger v_s), then T_s^* (T_h^*) is getting higher (smaller), FOPT is enhanced in this limit.

[1] The one-step EWPT ($\Omega_0 \to \Omega_h$) is the second order for the range in Fig. 1 (right). The one-step FOEWPT is realized for $m_s \gtrsim 400$ GeV with large λ_{sh} by the non-decoupling thermal loop effects even for $A_s = 0$ as discussed in Refs. [13, 15, 16, 22, 25].

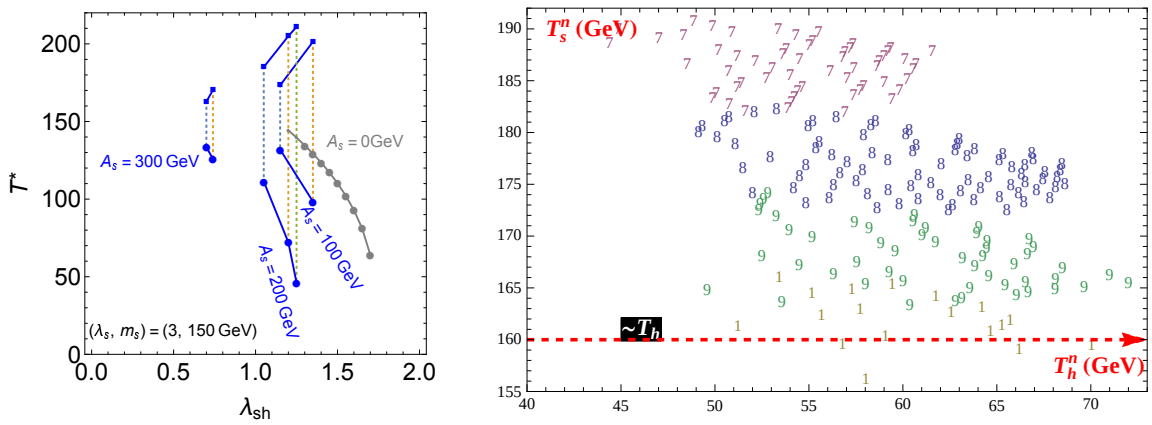

Figure 2: (Left) The two-step PT in the $\mu_s^2 > 0$ region as the function of λ_{sh}. The first- $\to$ first- order PT arises are shown for $(\lambda_s, m_s[\mathrm{GeV}]) = (3, 150)$ by taking $A_s[\mathrm{GeV}] = 100, 200, 300$ (blue lines). For each dashed line, the upper and the lower ends denote T_s^* and T_h^*, respectively. In these plots we just keep the points which give FOPT. (Right) The three-step EWPT in the $\mu_s^2 < 0$ region with $\lambda_{sh} = 0.24$, varying $\lambda_s = 0.7, 0.8, 0.9, 1.0$ which is labelled by numbers 7, 8..., respectively. Distributions of two FOPT temperatures, T_s^* and T_h^*; the red dashed line denotes T_h, the typical second order PT temperature for $\Omega_0 \to \Omega_h$.

4.2 Dark matter constraints

Constraints on DM properties are also displayed on the (A_s, λ_{sh}) plane in Fig. 1 (right). We used the micrOmegas v.4.3.2 [26] to calculate the thermal relic density σ_s and the DM-nucleon elastic scattering cross section $\Omega_s h^2$. The shaded blue regions have been excluded already by XENON1T [24] [2] except for the region of $\lambda_{sh} \lesssim 0.1$ or a sufficiently large $|A_s|$. By comparing the successful points of PT, we find that only the three-step PT can satisfy the current DM direct detection bound. In this case, the thermal relic density of the model which is normalized by the observed one $\Omega_{\mathrm{DM}} h^2 = 0.1199 \pm 0.0022$ [29] is predicted as $\Omega_s / \Omega_{\mathrm{DM}} \simeq 10^{-2}$. However, just like in the Z_2 model, it fails, at least being the dominant DM component because the relic density is suppressed owing to the large singlet-Higgs coupling required by SFOEWPT [12, 13]. Here the presence of a new coupling A_s still does not open the region $\lambda_{sh} \lesssim \mathcal{O}(0.01)$ that is necessary to accommodate correct DM relic density. We find that, in order to satisfy the condition of FOPT, the DM component should be at most about 1% of the total DM abundance.

4.3 Detectability of gravitational waves

Finally, we display the results on the $(\alpha, \widetilde{\beta})$ plane in the Fig. 3, with the experimental sensitivities of LISA [17, 30] and DECIGO [19] labelled by the shaded regions. The sensitivity regions of four LISA detector configurations described in Table I in Ref. [17] are denoted by "C1", "C2", "C3" and "C4". The expected sensitivities for the future DECIGO stages are labeled by "Correlation", "1 cluster" and "Pre" following Ref. [19]. The transition temperature T_* depends on the model parameters (see, Fig. 2) and the velocity of the bubble wall v_b is uncertain. Although the experimental sensitivities on the $(\alpha, \widetilde{\beta})$ depend on T_* and v_b, we take $T_* = 50$ GeV and $v_b = 0.95$ as a reference for the purpose of illustration.

[2] See also the recent results from LUX [27] and PandaX-II [28] experiments.

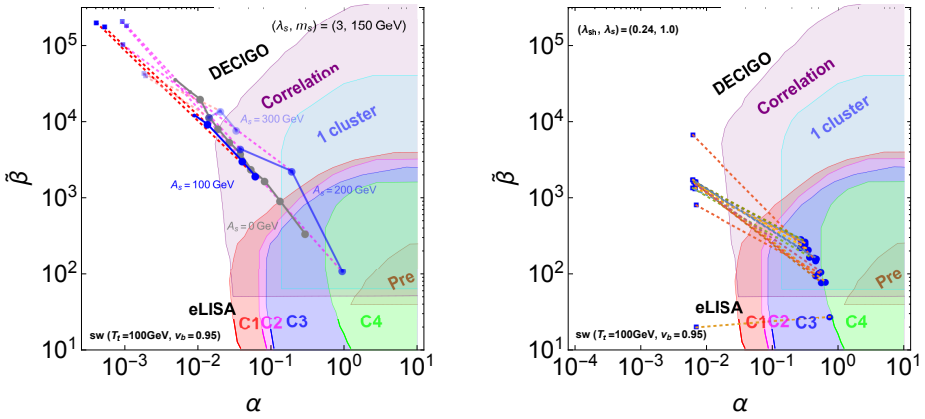

Figure 3: Detectability of GWs in the $(\alpha, \widetilde{\beta})$ plan from the two-step (first-first order) PT (left) and the three-step (first-second-first order) PT (right) which are corresponding to Fig. 2, respectively. The two FOPTs are labelled respectively by the square and circle points, connected by a dashed line. The expected sensitivities of LISA and DECIGO are set by using the sound wave contribution for $T_* = 100$ GeV and $v_b = 0.95$.

It is seen that typically one needs $\alpha \gtrsim \mathcal{O}(0.01)$ for the near future detection. However, the first source from $\Omega_0 \to \Omega_s$ with FOPT turns out to be undetectable since it always gives $\alpha \lesssim 0.01$. On the other hand, in particular in the three-step PT case, most of the parameter space can be covered for the other source of EWPT. One of the main reasons causing this difference is that the first-step happened at a relatively high temperature $T_s^* \gtrsim 160$ GeV, which typically is rather higher than the EWPT temperature $T_h^* \lesssim 100$ GeV; recalling that $\alpha \propto 1/T^4$, thus the first source is suppressed. A lower T_h^* also leads to smaller $\widetilde{\beta}$, which is determined by the PT temperature.

5. Conclusion

A potential barrier can be created during EWPT by the tree level effects due to a doublet-singlet mixing [5, 6, 7, 8, 9, 10, 11]. As a result, such models can be tested by the synergy between the measurements of various Higgs boson couplings at future collider experiments and the observation of GWs at future space-based interferometers as discussed in Refs. [10, 11]. In another implementation imposing unbroken discrete symmetry like Z_2 [7, 12, 13, 14, 15, 16], multi-step PT could utilize a tree level barrier. But generically the absence of mixing renders the tests at colliders difficult without taking enough large λ_{sh} coupling as discussed in Refs. [13, 15, 16, 22, 25]. In this paper, we have focused on such the nightmare scenario in the Z_3 symmetric single scalar model. Especially, the three-step PT produces two sources of GW in the model. Despite of the undetectability from the first-step in the near future, the other source from EWPT basically can be completely covered by LISA and DECIGO.

Acknowledgements

This work is based on the collaboration with Zhaofeng Kang and Pyungwon Ko. I would like to thank them for their support.

References

[1] Z. Kang, P. Ko and T. Matsui, JHEP **1802**, 115 (2018).

[2] V. A. Kuzmin, V. A. Rubakov, and M. E. Shaposhnikov, Phys. Lett. B155 (1985) 36; M. E. Shaposhnikov, Nucl. Phys. B287 (1987) 757-775.

[3] D. E. Morrissey and M. J. Ramsey-Musolf, New J. Phys. **14**, 125003 (2012).

[4] D. J. H. Chung, A. J. Long and L. T. Wang, Phys. Rev. D **87**, no. 2, 023509 (2013).

[5] S. Profumo, M. J. Ramsey-Musolf and G. Shaughnessy, JHEP **0708**, 010 (2007).

[6] A. Ashoorioon and T. Konstandin, JHEP **0907**, 086 (2009).

[7] J. R. Espinosa, T. Konstandin and F. Riva, Nucl. Phys. B **854**, 592 (2012).

[8] K. Fuyuto and E. Senaha, Phys. Rev. D **90**, no. 1, 015015 (2014).

[9] S. Profumo, M. J. Ramsey-Musolf, C. L. Wainwright and P. Winslow, Phys. Rev. D **91**, no. 3, 035018 (2015).

[10] P. Huang, A. J. Long and L. T. Wang, Phys. Rev. D **94**, no. 7, 075008 (2016).

[11] K. Hashino, M. Kakizaki, S. Kanemura, P. Ko and T. Matsui, Phys. Lett. B **766**, 49 (2017).

[12] J. M. Cline and K. Kainulainen, JCAP **1301**, 012 (2013).

[13] D. Curtin, P. Meade and C. T. Yu, JHEP **1411**, 127 (2014).

[14] V. Vaskonen, Phys. Rev. D **95**, no. 12, 123515 (2017).

[15] A. Beniwal, M. Lewicki, J. D. Wells, M. White and A. G. Williams, JHEP **1708**, 108 (2017).

[16] G. Kurup and M. Perelstein, Phys. Rev. D **96**, no. 1, 015036 (2017).

[17] C. Caprini *et al.*, JCAP **1604**, no. 04, 001 (2016).

[18] P. A. Seoane *et al.* [eLISA Collaboration], arXiv:1305.5720 [astro-ph.CO].

[19] S. Kawamura *et al.*, Class. Quant. Grav. **28**, 094011 (2011).

[20] V. Corbin and N. J. Cornish, Class. Quant. Grav. **23**, 2435 (2006).

[21] G. Belanger, K. Kannike, A. Pukhov and M. Raidal, JCAP **1301**, 022 (2013).

[22] K. Hashino, M. Kakizaki, S. Kanemura and T. Matsui, Phys. Rev. D **94**, no. 1, 015005 (2016).

[23] C. L. Wainwright, Comput. Phys. Commun. **183**, 2006 (2012).

[24] E. Aprile *et al.* [XENON Collaboration], Phys. Rev. Lett. **119**, no. 18, 181301 (2017).

[25] M. Kakizaki, S. Kanemura and T. Matsui, Phys. Rev. D **92**, no. 11, 115007 (2015).

[26] D. Barducci, G. Belanger, J. Bernon, F. Boudjema, J. Da Silva, S. Kraml, U. Laa and A. Pukhov, Comput. Phys. Commun. **222**, 327 (2018).

[27] D. S. Akerib *et al.* [LUX Collaboration], Phys. Rev. Lett. **118**, no. 2, 021303 (2017).

[28] X. Cui *et al.* [PandaX-II Collaboration], Phys. Rev. Lett. **119**, no. 18, 181302 (2017).

[29] P. A. R. Ade *et al.* [Planck Collaboration], Astron. Astrophys. **594**, A13 (2016).

[30] Data sheet by A. Petiteau, http://www.apc.univ-paris7.fr/Downloads/lisa/eLISA/Sensitivity/Cfgv1/StochBkgd/